Colloid Polym Sci 278:972–978 (2000)

SHORT COMMUNICATION

T. Hellweg
C. D. Dewhurst
E. Brückner
K. Kratz
W. Eimer

Colloidal crystals made of poly(*N*-isopropylacrylamide) microgel particles

Received: 26 July 1999
Accepted: 21 March 2000

T. Hellweg (✉)
TU Chemnitz, Institut für Physik
Materialforschung und Flüssigkeiten
09107 Chemnitz, Germany
e-mail: T.Hellweg@physik.tu-chemnitz.de

C. D. Dewhurst
Institut Laue-Langevin
Avenue des Martyrs
BP156, 38042 Grenoble Cedex 9, France

E. Brückner
Universität Essen
Institut für Umweltanalytik
Universitätsstrasse 3-5, 45141 Essen
Germany

K. Kratz · W. Eimer
Universität Bielefeld
Fakultät für Chemie
Physikalische Chemie 1
33615 Bielefeld, Germany

Abstract Poly (*N*-isopropylacrylamide) microgel particles are found to form colloidal crystals similar to those occurring in typical hard-sphere colloids like poly(methylmethacrylate) beads. Samples made of particles with different cross-linker concentrations are investigated and their deswelling ratio is determined using dynamic light scattering. Small-angle neutron scattering data are also presented and analysed in terms of a face-centred-cubic crystal structure. The characteristic length, a, of the elementary cell is found to be 535 ± 16 and 495 ± 15 nm for the two systems investigated. This leads to particle radii of 189 ± 6 and 175 ± 5 nm, respectively. These values compare well to the radii determined using several different methods.

Key words Colloids · Microgel · Face-centred-cubic lattice · Small-angle neutron scattering · Light scattering

Introduction

Recently, gelling polymer systems have attracted a great deal of attention [1–9]. Firstly, due to their use in an increasing number of technical applications, such as storage or transport media, and, secondly, due to the considerable lack of theoretical understanding of these systems. Thermosensitive poly (N-isopropylacrylamide) (PNIPA) copolymers were intensely studied, due to the observation of a temperature-dependent volume phase transition [4]. This makes the material a possible candidate for the construction of artificial muscle and micromachines. Furthermore, the bioadhesive properties of these materials suggest that NIPA copolymers may be appropriate for applications as drug carriers. Recently, significant attention has been given to colloidal microgel particles based on the same material [10–14]. These can be obtained nearly monodisperse and can be prepared with a wide range of colloidal sizes (typically 50 nm up to 1 μm), making them attractive as potential drug carriers, rather than their macroscopic homologues. Furthermore, they are easier to study due to their shorter equilibration times when external stimuli, such as temperature, ionic strength or pH, are changed. Since the interaction between colloidal particles is of importance for a vast number of natural and industrial processes, PNIPA microgel particles might provide an interesting model system to study ordering phenomena

and aggregation in colloidal systems. The interaction potential controlling these ordering phenomena depends on the degree of cross-linking and can be varied from soft-polymer-like to hard-sphere-like [15]. Another important factor which has an impact on the formation of crystalline or glassy phases in colloidal systems is the size and shape polydispersity. Due to the preparation procedure microgels can be obtained with very low polydispersities (usually 10% or lower) and are therefore ideal model systems for study. Such colloidal crystals with tunable characteristic length scales might be useful as templates for nanocasting [16, 17] to design, for example, photonic band-gap materials.

However, not only the internal structure, the polydispersity, and the size, but also the conditions during synthesis play an important role because these influence the surface charge of the particles obtained. Here, we present data for particles with very low surface charge. This is different compared to other studies [15].

For a liquid of hard-sphere particles, "freezing" takes place at volume fractions, ϕ, higher than about 0.494 [18–20]. For soft spheres the crystallisation occurs at slightly higher values ($\phi = 0.6$) [15]. NIPA microgel particles allow this particle volume fraction to be reached even at low polymer concentrations since the particles are able to swell, leading to an increase in volume of up to a factor of 10 [21].

In this contribution we focus on NIPA microgels with two different cross-linker concentrations (2% N,N′-methylenebisacrylamide, BIS, and 10% BIS).

Materials and methods

Synthesis of PNIPA microgels

NIPA, BIS, and potassium persulfate (KPS) were obtained commercially from Sigma-Aldrich. All chemicals were reagent grade and were used without further purification. The microgel preparation is based on the procedure described by Pelton and Chibante [22]. For the synthesis of the particles used here we employed a conventional stirring technique as described elsewhere [11]. NIPA (1.25 g, 10.05 mmol) and the desired amounts of BIS (1.00 mmol and 0.20 mmol, respectively) were dissolved in 100 ml triple-distilled, degassed water. The synthesis was performed under a nitrogen atmosphere to exclude oxygen. After heating the solution to 343 K, 3.6 μmol KPS were added to start the polymerisation. The mixture became turbid and the reaction proceeded for 4 h at constant temperature. Then the microgel suspension was cooled for 12 h under continuous stirring. The final step of the preparation involves extensive dialysis for 20 days against double-distilled water in order to remove unreacted monomers and other low-molecular-weight impurities.

Dynamic light scattering

The dynamic light scattering (DLS) experiments were performed using a classical goniometer setup with pinhole collimation (ALV, Langen, Germany) and a digital correlator (ALV5000). As a light source we employed an argon ion laser (Coherent, Innova 90) operated at a wavelength of 488 nm in single mode and at a constant output power of 400 mW. The samples were filled into dust-free sample cells and centrifugated at about 800g to sediment spurious amounts of dust which may be present. The samples were then placed in a toluene-containing index-matching bath and were regulated at the desired temperature with a precision of ± 0.1 K.

Small-angle neutron scattering

Small-angle neutron scattering (SANS) measurements were made using the D11 small-angle machine at the high-flux reactor of the ILL in Grenoble (further instrumental details are given in the respective publications of the ILL). The incident neutron wavelength was 10°. The multidetector data were radially averaged about the beam centre and the background counting rate was substracted from the data. To get appropriate contrast for the neutron scattering experiments the previously freeze-dried samples were resuspended in heavy water (isotopic purity 99.9%, Eurisotop).

Results and discussion

Size and swelling behaviour

Both types of colloidal microgel particles were characterised by DLS [23]. All DLS experiments were performed in the dilute regime where interparticle interaction is negligible. For more details of the DLS experiments see Refs. [11, 13]. The radii and the polydispersities of the samples were computed from the z-averaged relaxation rate, $\bar{\Gamma}$, of the correlation functions as obtained from a CONTIN [24, 25] analysis. A second-order cumulant fit [26] of the data led to the same result. For centre-of-mass diffusion $\bar{\Gamma}$ is proportional to the square of the magnitude of the scattering vector

$$Q = \frac{4\pi n}{\lambda} \sin\left(\frac{\theta}{2}\right) \quad . \tag{1}$$

In this equation λ is the wavelength of the incident radiation, n the refractive index, and θ the scattering angle.

The proportionality constant is the translational diffusion coefficient, which can be used to compute the hydrodynamic radius, R_h, by applying the Stokes–Einstein equation

$$D_0 = \frac{kT}{6\pi\eta R_h} \quad , \tag{2}$$

with the solvent viscosity η, the absolute temperature T, and the Boltzmann constant k. At 288.2 K the hydrodynamic radii are 275 ± 14 and 258 ± 13 nm, respectively. For both samples the polydispersity was found to be 10% or lower.

The swelling behaviour of the particles was subsequently investigated by increasing the temperature in steps of 1 K. When the sample reached thermal equilibrium correlation functions were recorded at a fixed angle of 90°. The swelling curves obtained are shown in Fig. 1.

The transition temperatures obtained from the minimum in the numerical derivatives of the data are $T = 303.7$ K for 2% BIS and $T = 307.3$ K for 10% BIS. Higher cross-linker content leads to a higher transition temperature. In comparison to the swelling curves obtained by other groups [15] we do not observe a significant decrease in the hydrodynamic radius before the phase transition temperature is reached. Within experimental error the radii are constant up to 298.1 K for 2% BIS and up the 301 K for 10% BIS. On the other hand, the preparation of the microgels investigated here is different from the procedures used in other studies (no surfactant, nearly 2 orders of magnitude lower starter concentration). The difference may explain the slightly different low-temperature behaviour in comparison to Ref. [15]. The swelling/deswelling ratio, α, can be computed from the swelling curves using the equation

$$\alpha = \frac{V_{\text{collapsed}}}{V_{\text{swollen}}} = \left(\frac{R_{\text{h}}^{313.2\text{K}}}{R_{\text{h}}^{288.2\text{K}}}\right)^3 . \quad (3)$$

For the sample containing 2% BIS this leads to $\alpha = 0.118$ and for the sample containing 10% BIS we find $\alpha = 0.312$.

Additionally, the particles were characterised in dilute solution by static light scattering (SLS) and SANS. These methods provide knowledge of the radius of gyration of the particles. Real-space imaging techniques such as video microscopy [27] and electron microscopy were also used to characterise the samples [28], resulting in the parameters for the swollen particles listed in Table 1. The value obtained using electron microscopy is slightly lower than the other values, since the particles were placed on a glass support and then dried at room temperature before being sputtered with gold, which is necessary for electron microscopy. This means the external chains collapse. The values given are corrected for the thickness of the gold layer. The radii measured for the shrunken state (at 313.2 K) are given in Table 2. There is no significant difference between the size of the shrunken particles in solution and the freeze-dried ones. Video microscopy was also used to monitor the processes occurring in a concentrated solution of a 10% BIS sample. The results are shown in Fig. 2. The first picture is taken in the molten state of the system at 308 K. On subsequent cooling the sample begins to order and finally ends up in an obviously polycrystalline state (Fig. 2f, $T = 290$ K). We also made dark-field microscope measurements, which indicate grain boundary features within the crystalline areas (images not shown). Since only the two-dimensional structure can be observed using these methods we performed SANS experiments on concentrated samples to obtain further information on the crystal structure.

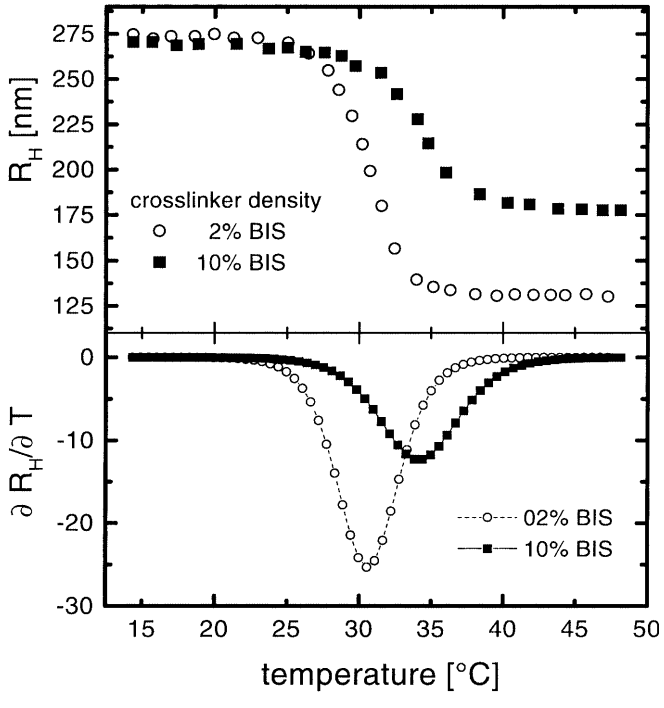

Fig. 1 Swelling curves of the two colloidal microgels investigated in this study. The lower part of the figure shows the numerically calculated derivatives, which we use to determine the volume phase transition temperature

Determination of the volume fraction

The volume fractions of the samples prepared for the SANS experiments can be estimated by applying scaling laws [29], which provide a relationship between the radius of gyration, R_{g}, and the molecular weight, M.

Table 1 Radii of the microgel particles as determined by different experimental techniques. All data given were measured for particles in the swollen state at 288.2 K. The values given for R^{REM} were obtained for samples dried in air

	2% BIS	10% BIS
$R_{\text{h}}^{\text{DLS}}$ (nm)	275	258
$R_{\text{g}}^{\text{SLS}}$ (nm)	233	212
$R_{\text{g}}^{\text{SANS}}$ (nm)	220	220
R^{REM} (nm)	180	185
R^{Video} (nm)	–	225

Table 2 Radii of the microgel particles as determined by different experimental techniques. All data given were measured for particles in the shrunken state at 313.2 K

	2% BIS	10% BIS
$R_{\text{h}}^{\text{DLS}}$ (nm)	135	175
$R_{\text{g}}^{\text{SLS}}$ (nm)	141	171

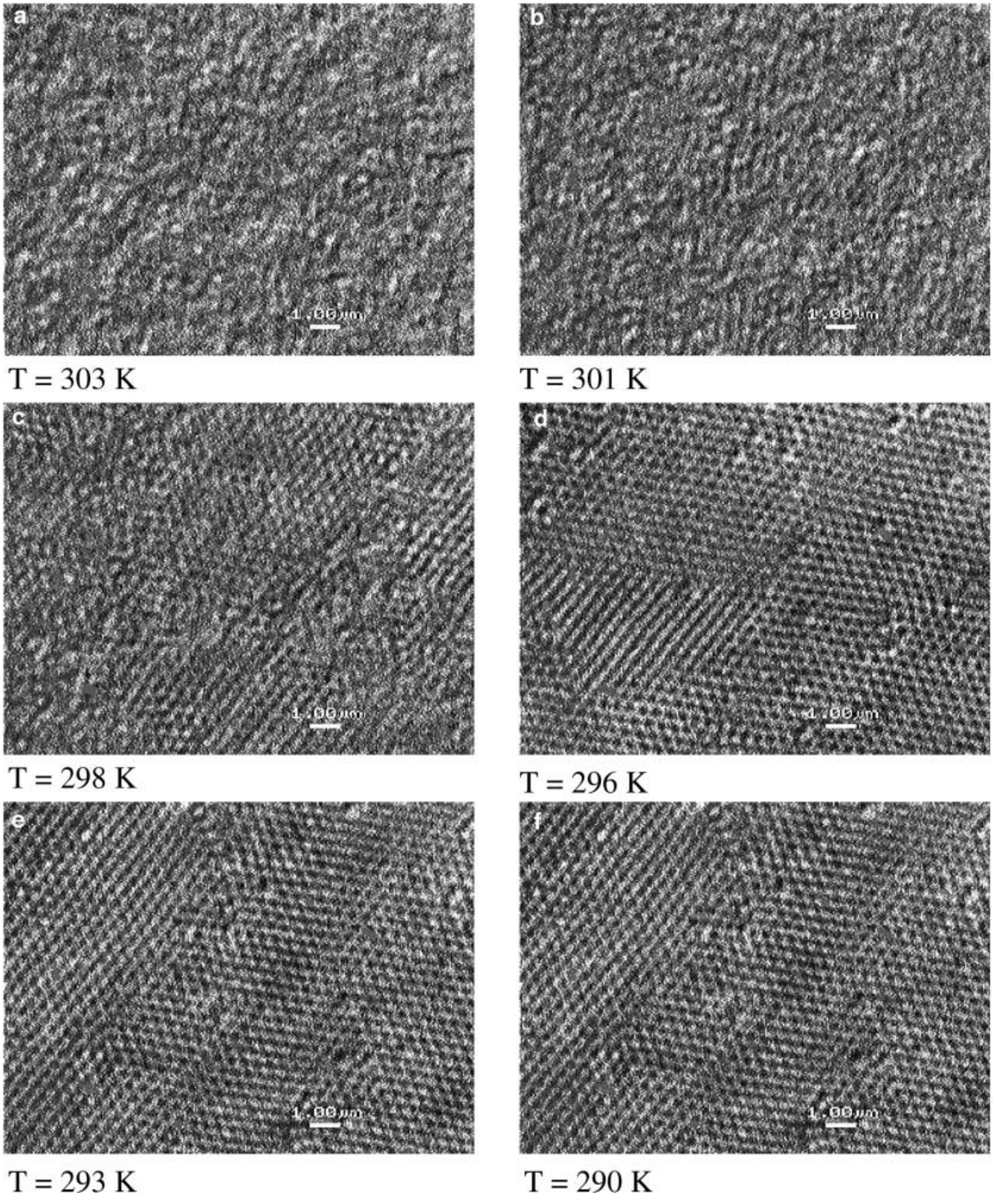

Fig. 2 Video microscopy images for a sample prepared with 10% cross-linker at six different temperatures. The crystal formation is obvious from these images

$$\langle R_g \rangle \propto M^{\frac{1}{3}} \Rightarrow \langle R_g \rangle^3 \propto V_{\text{particle}} \propto M \quad . \tag{4}$$

From this it follows that the particle volume fraction is directly proportional to the weight concentration of the freeze-dried polymer. From electron micrographs and SLS experiments we know that the radius of the freeze-dried microgel particles is equal to the hydrodynamic radius of the particles in the shrunken state. Knowing the deswelling ratio, α, we can now calculate the volume fractions in our samples at low temperature (swollen state). A second way to obtain information about the effective volume fraction is to use the relation $\phi_{\text{eff}} = kc$ [15]. Senff and Richtering determined a k-value of 1.2 for their NIPA microgels with ≈2% cross-linker. Following the first approach, the particle volume fraction in the samples measured here is $\phi \approx 0.89 \pm 0.09$ for the 2% cross-linker (BIS) samples and $\phi \approx 0.62 \pm 0.06$ for the 10% cross-linker (BIS) samples. These volume fractions correspond to polymer concentrations of 113 and 185 g/l. Using the second approach with $k = 1.2$ we get $\phi \approx 1.07 \pm 0.11$ and $\phi = 0.74 \pm 0.07$, respectively. The errors are calculated in both cases under the assumption that the freeze-dried particles still contain approximately 10 wt% of residual water. Both estimations lead to values of $\phi \geq 0.6$, which is the threshold for the crystallisation of soft spheres. The samples almost immediately begin to crystallise when filled into quartz cells (Hellma) and therefore begin to show birefringence. This effect is displayed in Fig. 3, where suspensions of the colloidal particles are shown between glass plates.

Colloidal crystals

Concentrated samples of the two different microgels were investigated using SANS at very low Q ranges (10^{-2} nm^{-1}; comparable to light scattering). For a colloidal dispersion of hard spheres the scattered intensity, I(Q), observed in a SANS experiment is given by

$$I(Q) = NS(Q)P(Q) \quad , \tag{5}$$

where $P(Q)$ is the particle structure factor, $S(Q)$ the inter-particle structure factor, N the particle number density, and Q the magnitude of the scattering vector. Assuming that the particle structure factor $P(Q)$ does not depend on concentration, for low polydispersities it is possible to extract the structure factor of a concentrated colloidal solution or colloidal crystal by dividing $I(Q)_{\text{conc.}}$ by $I(Q)_{\text{dil.}}$ [14]. This approach can be applied here since the particles have very low polydispersities and the radius does not change significantly with concentration. For the very dilute light scattering samples we find the same radius of gyration as for the "dilute" SANS samples, where the concentration was already increased by a factor of 10^5 to get sufficiently high scattering intensity at low Q (Table 1).

Using the approach described here, we investigated the two different colloidal microgels previously characterised by DLS. The scattering profiles for 2% cross-linker are shown for a dilute solution (0.85 wt% polymer) and for a concentrated sample (8.5 wt% polymer) in Fig. 4 and those for 10% cross-linker are shown in Fig. 5. The interparticle structure factor obtained by division of the two measured scattering

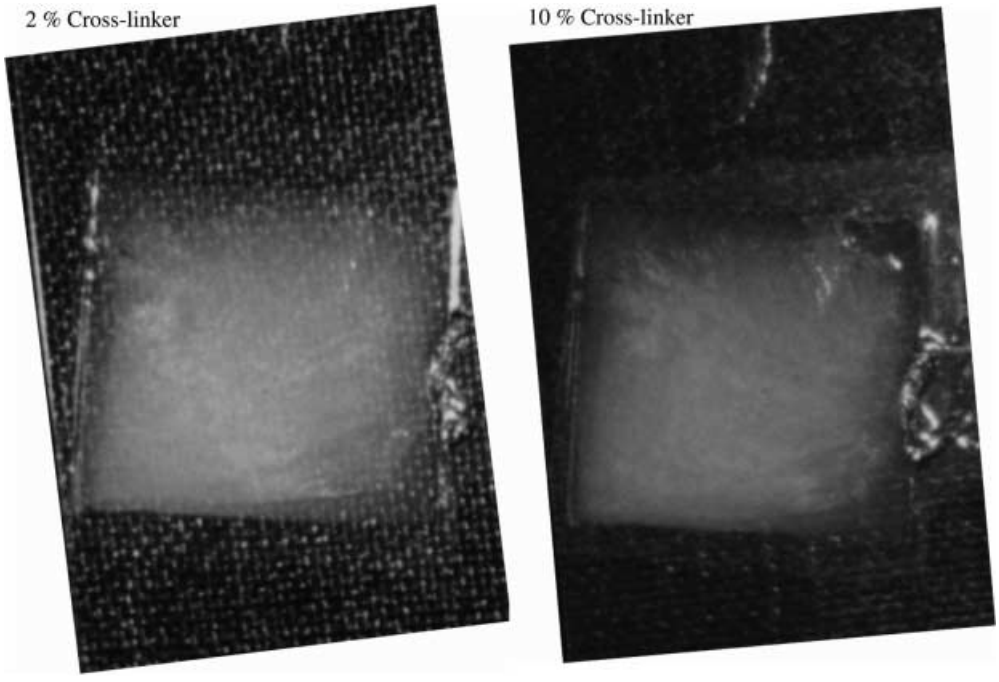

Fig. 3 Crystallized samples between glass supports

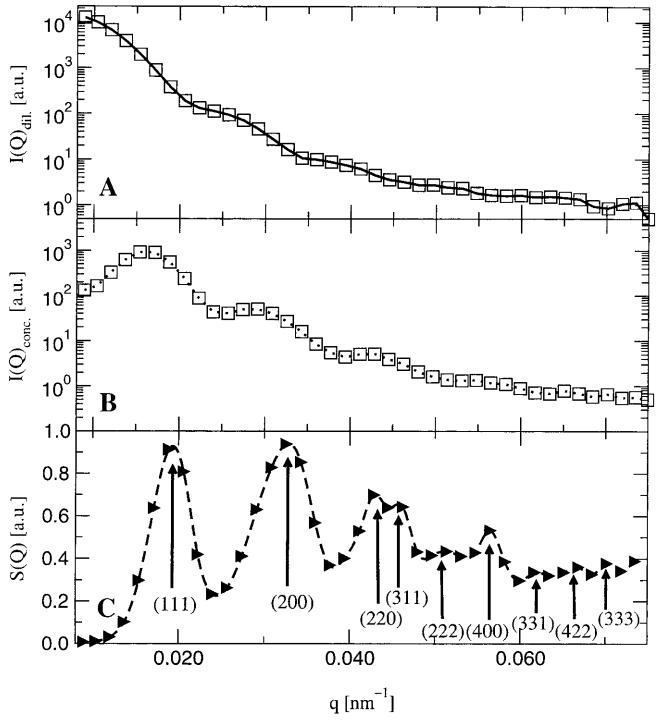

Fig. 4 2% cross-linker: (A) Scattering profile for a dilute solution of the microgel particles; (B) Scattering profile for a concentrated crystallised sample; (C) $I(Q)_{\text{conc.}}/I(Q)_{\text{dil.}}$. In (C) several Bragg peaks are observable. The given (hkl) values arise from an interpretation in terms of the fcc latice

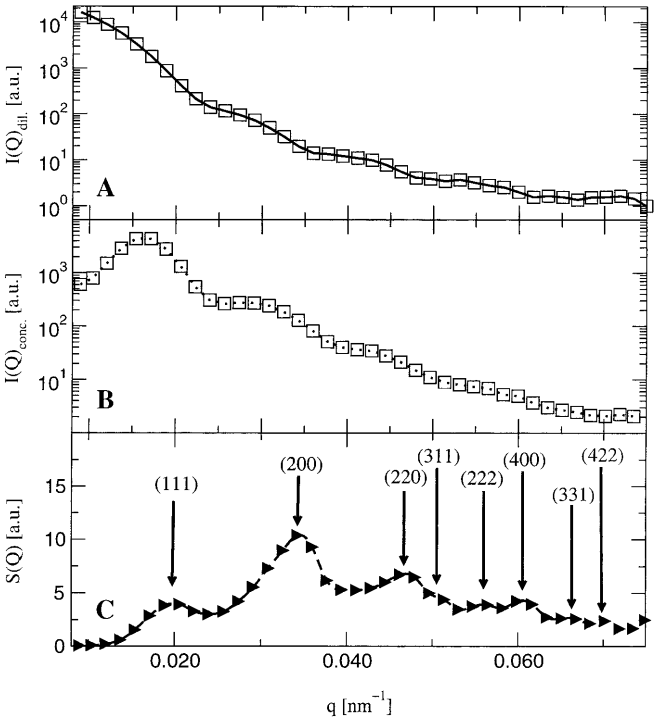

Fig. 5 10% cross-linker: (A) Scattering profile for a dilute solution of the microgel particles; (B) Scattering profile for a concentrated crystallised sample; (C) $I(Q)_{\text{conc.}}/I(Q)_{\text{dil.}}$. In (C) several Bragg peaks are observable

profiles shows several Bragg peaks. For a face-centred-cubic (fcc) lattice those reflections are observable which have only odd or only even reciprocal lattice vectors h, k, and l [30]. Therefore, assuming a fcc structure the cubic lattice constant a can be obtained from the peak positions according to

$$a = d_{(hkl)}\sqrt{h^2 + k^2 + l^2}\ , \tag{6}$$

where $d_{(hkl)} = 2\pi/Q_{(hkl)}$. The raw data and the peaks obtained are displayed in Fig. 4. Plotting the Q_{hkl} values versus $2\pi\sqrt{h^2 + k^2 + l^2}$ leads to a straight line with slope $1/a$. For 2% cross-linker the linear fit yields $a = 535 \pm 16$ nm (Fig. 6). The (1 1 1) peak was omitted in the analysis because it is misplaced due to the interference with the maximum of the liquid structure factor, $S(Q)$. $S(Q)$ still contributes to the scattering because crystallisation occurred at the surface of the sample cell and there are still some liquidlike regions in the neutron beam which perturb the scattering; however, this value leads to a radius of 189 ± 6 nm. This is in good agreement with the particle size as previously estimated from SLS and SANS ($a/\sqrt{2} \approx 2R_g$). For 10% BIS we used a similar approach as also shown in Fig. 6. Again assuming a fcc structure we find $a \approx 495 \pm 15$ nm from the linear fit of $Q_{(hkl)}$ versus $2\pi\sqrt{h^2 + k^2 + l^2}$. This value for a is once more in agreement with that predicted

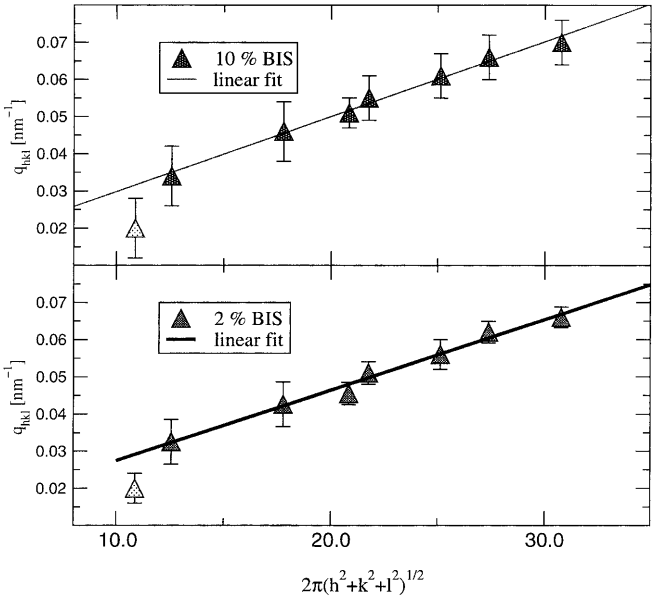

Fig. 6 In this figure the linear dependence of $Q_{(hkl)}$ on $2\pi\sqrt{h^2 + k^2 + l^2}$ is shown for both microgels. For 10% BIS the points show slightly stronger deviations from the linear fit

from the radius of gyration of the colloidal microgel particles as obtained from SLS. Figure 2f corresponds to the samples investigated by SANS.

Conclusions

From the results presented we can conclude that the PNIPA microgel particles are an ideal model system for the study of colloidal crystallisation. Even at low cross-linker concentration (''softer'' particle) the colloidal particles crystallise like hard-sphere liquids. The cross-linker content and, hence, the internal structure of the particles do not appear to have a significant influence on the colloidal crystals formed. The SANS peak positions are described well by a fcc lattice. Furthermore, the lattice parameter, a, calculated for a fcc structure is found to be close to the value predicted from the radius of gyration of the particles in dilute solution. This indicates that the swelling behaviour of the particles does not differ significantly in the dilute or concentrated regime. From the peak positions in the interparticle structure factor we propose that the microgel particles order into a fcc structure for both samples. Future studies are planned to follow the kinetics of crystallisation in these systems and to investigate the melting by means of SANS.

References

1. Hecht A-M, Duplessix R, Geissler E (1985) Macromolecules 18:2167–2173
2. Pusey PN, van Megen W (1989) Physica A 157:705–741
3. Horkay F, Hecht A-R, Mallam S, Geissler E, Rennie AR (1991) Macromolecules 24:2896–2902
4. Shibayama M, Tanaka T, Han CC (1992) J Chem Phys 97:6829–6841
5. Shibayama M, Tanaka T, Han CC (1992) J Chem Phys 97:6842–6854
6. Geissler E, Horkay F, Hecht A-M (1993) Phys Rev Lett 71:645–648
7. Shibayama M, Tanaka T (1995) J Chem Phys 102:9392–9400
8. Stellbrink J (1997) Complex dynamics in the vicinity of the sol–gel transition. Nonergodic and fractal behaviour of polyacrylamide gels. Verlag Mainz, Wissenschaftsverlag
9. Ikkai F, Shibayama M, Han CC (1998) Macromolecules 31:3275–3281
10. Crowther HM, Saunders BR, Mears SJ, Cosgrove T, Vincent B, King SM, Yu G-E (1999) Colloids Surf A 152:327–333
11. Kratz K, Eimer W (1998) Ber Bunsenges Phys Chem 102:848–854
12. Dingenouts N, Nordhausen Ch, Ballauff M (1998) Ber Bunsenges Phys Chem 102:1594–1596
13. Kratz K, Hellweg T, Eimer W (1998) Ber Bunsenges Phys Chem 102:1603–1608
14. Bartsch E, Kirsch S, Lindnen P, Scherer T, Stölken S (1998) Ber Bunsenges Phys Chem 102:1597–1602
15. Senff H, Richtering W (1999) J Chem Phys 111:1705–1711
16. Svec F, Frechet JMJ (1996) Science 273:205–211
17. Holland BT, Blanford CF, Stein A (1998) Science 281:538–540
18. Dhont JKG, Smits C, Lekkerkerker HNW (1992) J Colloid Interface Sci 152:386–401
19. Segre PN, Meeker SP, Pusey PN, Poon WCK (1995) Phys Rev Lett 75:958–961
20. Heymann A, Stipp A, Sinn C, Palberg T (1998) J Colloid Interface Sci 207:119–127
21. Kratz K, Hellweg Th, Eimer W (1999) Structural changes in NIPA microgel particles as seen by SANS, DLS and EM techniques, submitted
22. Pelton RH, Chibante P (1986) Colloids Surf 20:247
23. Berne BJ, Pecora R (1976) Dynamic light scattering. Wiley, New York
24. Provencher SW (1982) Comput Phys Commun 27:213–217
25. Provencher SW (1982) Comput Phys Commun 27:229–242
26. Koppel DE (1972) J Chem Phys 57:4814–4820
27. Inoue S (1986) Video Microscopy. Plenum, New York
28. Kratz K (1999) PhD thesis. University of Bielefeld
29. de Gennes PG (1979) Scaling concepts in polymer physics. Cornell University Press, Ithaca
30. Kleber W (1983) Einführung in die Kristallographie, 15th edn. VEB Verlag der Wissen-Schaffem, Berlin
31. Hamley IW, Pople JA, Diat O (1998) Colloid Polym Sci 276:446–450